

Coronal heating and photospheric turbulence parameters: observational aspects

V.I. Abramenko

Big Bear Solar Observatory, 40386 N. Shore Lane, Big Bear City, CA 92314; avi@bbso.njit.edu

Alexei A. Pevtsov

National Solar Observatory, Sunspot, NM 88349; apevtsov@nso.edu

P. Romano

Dipartimento di Fisica e Astronomia, Università di Catania, via S. Sofia 78, 95125 Catania, Italy

ABSTRACT

In this study, the soft X-ray luminosity of the solar corona, measured by the *Yohkoh* spacecraft for 104 well developed and decaying active regions, is compared to the magnetic field parameters determined from SOHO/MDI high resolution magnetograms. We calculated and compared the following parameters: i) two area-independent characteristics of the magnetic field: index (α) of the magnetic power spectrum, $E(k) \sim k^{-\alpha}$ and the magnetic energy dissipation rate ($\bar{\varepsilon}/\eta$) which is a proxy for the energy of random footpoint motions induced by turbulent convection in the photosphere and below; ii) four area-independent parameters of the soft X-ray emission: the area-normalized flux in *Yohkoh* Al.1 and AlMgMn channels, the emission measure and temperature of the coronal plasma. Here we report that the area-normalized soft X-ray flux correlates with both the power index α (Pearson correlation coefficient $\rho = 0.72/\text{Al.1}$ and $0.73/\text{AlMgMn}$) and the magnetic energy dissipation rate $\bar{\varepsilon}/\eta$ ($\rho = 0.68/\text{Al.1}$ and $0.70/\text{AlMgMn}$). Also, both magnetic parameters are well-correlated with the logarithm of the emission measure ($\rho = 0.72$) and the logarithm of temperature ($\rho = 0.59/\alpha$ and $0.63/\bar{\varepsilon}/\eta$). Our results present strong observational support to those coronal heating models that rely on random footpoint motions as an energy source to heat the corona above active regions.

Subject headings: Sun: coronal heating; magnetic field

1. Introduction

Since Fisher’s et al. (1998) study, solar magnetic fields were proved to play a key role in the heating of the solar corona. The authors demonstrated that a close connection exists between the unsigned magnetic flux and the total X-ray luminosity of the corona above 333 active regions. The observed linear functional dependency is in agreement with magnetic dissipation coronal heating models, such as the “minimum current corona” (MCC) model (Longcope 1996). This relationship was later confirmed by several studies (e.g., Pevtsov et al., 2003; Schrijver & Title 2005 and references therein). Although there is still no general agreement on the physical mechanism that can be responsible for this relationship, the functional dependency is successfully implemented in the modeling of the observed X-ray corona above active regions (Lundquist et al., 2004, Schrijver et al., 2004).

The most important requirement for any model of coronal heating is the capability to provide the necessary energy flux on the order of $10^7 \text{ erg cm}^{-2}\text{s}^{-1}$ in active regions and $3 \times 10^5 \text{ erg cm}^{-2}\text{s}^{-1}$ in quiet sun (Withbroe & Noyes 1977) to efficiently heat the corona. It has recently been suggested (see, e.g., recent review by Klimchuk 2006) that the most probable source of this energy is random motions of footpoints of magnetic flux tubes induced by turbulent convection at the surface of, and just below, the photosphere. Displacement of the footpoints results in the build up of stress in the magnetic field (DC heating) and/or waves (AC heating). Klimchuk (2006) argued that, as of today, the DC heating models are the most plausible and most compatible with observations. These models include the original Parker braiding idea (Parker 1988) and a new development of that idea by Priest et al. (2002) which takes account that the coronal magnetic field arises from the highly fragmented magnetic carpet.

The energy flux, that can be supplied by the footpoint motions, can be estimated with the Poynting flux (Parker 1979, 1988; Fisher et al. 1998; Dahlburg et al. 2005) as

$$F = -\frac{1}{4\pi} B_h B_v V_h, \quad (1)$$

where B_v and B_h are the vertical and horizontal components of the magnetic field and V_h is the horizontal velocity of the footpoints. Although this formula is very useful in modeling, it is rather difficult to utilize in a statistical study because reliable transverse magnetic and velocity fields measurements are not readily available. The energy flux associated with random footpoint motions can also be calculated by other means. In general, the photospheric plasma can be considered as a turbulent medium. In this case, solar magnetic fields embedded in the plasma are known to be confined to a conglomerate of thin vertical flux tubes (Stenflo & Holzreuter 2002 and references therein). This confined magnetic field diffuses in a turbulent flow, via random motions of footpoints, in the same way that a scalar field

does (Parker 1979; Petrovay & Szakaly 1993). The presence of turbulent conditions in the photosphere is evident from magnetic power spectra that exhibit the power law in the range of spatial scales of 3 – 10 Mm (Abramenko 2005). With this assumption in mind, one can make use of a passive scalar dissipation technique (Monin & Yaglom 1975) and calculate the magnetic energy dissipation rate on the basis of only the vertical component of the magnetic field. If random footpoint motions are indeed responsible for coronal heating, the magnetic energy dissipation rate (calculated per unit volume per unit time) should be proportional to certain area-normalized parameters of coronal X-ray luminosity.

In this Letter, we present results of a statistical comparison of the magnetic power spectra and magnetic energy dissipation rate versus the coronal soft X-ray flux, temperature and emission measure. In Section 2, we describe our data selection routine and the quantities analyzed. Section 3 reports the results of the correlation analysis, performed for 104 active regions, and presents estimations of the coronal heating flux. Concluding remarks are summarized in Section 4.

2. Analyzed data and quantities

2.1. Selection of active regions

We will focus on stable and decaying active regions only. All emerging sunspot groups were excluded from the study because earlier reports have described an unusual behavior of the power spectrum in emerging active regions (Abramenko 2005).

Active regions were drawn from a two-year time interval from Jan 2000 till Dec 2001. This time period includes the maximum of solar cycle 23 and was extensively observed by the soft X-ray telescope (SXT) on board *Yohkoh* (Tsuneta et al. 1991) and the Michelson Doppler Imager (MDI) on board the Solar and Heliospheric Observatory (Scherrer et al., 1995).

Selection of the active regions was based on several criteria. First, we initially chose all of the regions that were entirely located inside the field of view of the high resolution MDI magnetograms. Next, out of all of the chosen active regions, we selected only those active regions for which SXT data were available at least in one SXT channel (Al 0.1 μ m, thereafter Al.1, or AlMgMn-sandwich filters) in a 2-hour time window, centered at the time the magnetogram was obtained. When the SXT data were available in both Al.1 and AlMgMn filters, within that same time window, we selected those pairs of Al.1–AlMgMn images that were taken within 5 minutes of each other. We discarded all active regions for which the *Yohkoh* measurements were made during flaring periods, as reported by the

SolarGeophysical Data. Following this selection scheme, we choose total of 104 active regions. In this data set, Al.1 SXT images were available for 85 active regions, AlMgMn images for 103 ARs and 75 active regions had SXT data available in both the Al.1 and AlMgMn filters. Note that the number of active regions observed with both filters is smaller than the total number in either filter, due to the 5-minute time difference criterion between Al.1 and AlMgMn observations.

2.2. Magnetic field data and parameters

The high resolution MDI data were recorded with a spatial resolution of 1.25 arcsec and a corresponding pixel size of 0.58×0.58 arcsec (Scherrer et al., 1995). All active regions were located near the center of the solar disk, so that the projection effect in the line-of-sight magnetograms is negligible. This fact allowed us to consider the line-of-sight component of the magnetic field to be normal to the solar surface and it is denoted hereafter as B_z .

The first magnetic parameter we analyzed is the index, α , of the power spectrum $E(k) \sim k^{-\alpha}$ of the B_z component. The power spectrum was calculated by integrating, in the wavenumber space, the square of the two-dimensional Fourier transform of B_z . This technique, as well as examples of spectra for different types of active regions, are described elsewhere (Abramenko et al., 2001; Abramenko 2005). In the range of spatial scales $r > 3$ Mm, the slope of the power spectrum is not affected by noise and spatial resolution and the influence of large sunspots on the slope of the power spectrum, at spatial scales $r < 10$ Mm, is negligible (Abramenko et al. 2001; Abramenko 2005). Therefore, the spatial range $\Delta r = (3 - 10)$ Mm was selected as a linear interval where the power index was determined for all of the active regions in this study. The magnitude of α , in this study, varies between 1.3 and 2.5 (see Figure 1), and the calculation errors do not exceed ± 0.05 .

The second variable we analyzed is the magnetic energy dissipation rate normalized by the magnetic diffusivity, $\bar{\varepsilon}/\eta$. From the definition of the dissipation field of a passive scalar (Monin & Yaglom 1975) we can present the magnetic energy dissipation rate $\bar{\varepsilon}$ per unit volume per unit time as:

$$\bar{\varepsilon} = \eta \overline{\left(\left(\frac{dB_z}{dx} \right)^2 + \left(\frac{dB_z}{dy} \right)^2 \right)} \equiv \eta \overline{w(x, y)}, \quad (2)$$

where η is the magnetic diffusion coefficient. $\bar{\varepsilon}/\eta$ can be calculated from the observed B_z by averaging the dissipation $w(x, y)$ over the area of an active region, so that

$$\bar{\varepsilon}/\eta = \int dA w(x, y) / Area. \quad (3)$$

Here, the errors in the calculation of $\bar{\varepsilon}/\eta$, which can be introduced by noise and the differentiation routine, do not exceed 8-12%.

Note, that $\bar{\varepsilon}$ represents the amount of magnetic energy that cascades along the power spectrum, starting from the large scale portion of the spectrum. This input of energy occurs via, e.g., new flux emergence, and cascades down toward the smaller scales, where magnetic elements dissipate the magnetic energy due to resistivity. The magnitude of $\bar{\varepsilon}$ can also be estimated from the large-scale characteristics of a turbulent flow (Monin & Yaglom 1975):

$$\bar{\varepsilon} \simeq \frac{\Delta v_{\perp} \cdot (\Delta B_z)^2}{L}, \quad (4)$$

where Δv_{\perp} and ΔB_z are typical increments of the transverse footpoint velocity and the magnetic field on the scale L , that corresponds to the spatial scales of energy input. Equation (4) shows that the increase of the transverse velocities results in a gain of magnetic energy that cascades along the spectrum and, eventually, dissipates at small scales. That is to say, that $\bar{\varepsilon}/\eta$ can serve as a proxy for the energy of random footpoint motions.

Both the power index, α , and the magnetic energy dissipation rate, $\bar{\varepsilon}/\eta$, do not depend on the area of an active region.

2.3. Soft X-ray data and parameters

In the present study, we use full-frame desaturated (SFD) SXT images. The exposure time of these images is normalized, and uniform, throughout the data set. One drawback of SFD images is that they are logarithmically scaled and saved in a byte format. As a result, there is a slight increase in the roundoff errors for weak irradiances, as well as the complete loss of negative values. Stronger irradiances (i.e., the majority of the pixels in a typical image of an active region) are not affected by this effect. Besides, computation of the integrated parameters, averaged over a large number of pixels as is done in this study, further mitigates this problem.

The data were reduced using standard *Yohkoh* software (Freeland & Handy 1998) including correction for the telescope point-spread function (PSF). We used the software's default PSF, which consists of the core of the delta-function and the scattering wings, as determined from observations of several X-ray flares that were behind the limb. By using heliographic coordinates of the center of an active region and the size of the magnetogram, we selected the corresponding sub-image in the SXT data. We employed these sub-images to calculate the average (over a magnetogram's area) X-ray flux observed in the Al.1 (f1_{ave}) and AlMgMn (f2_{ave}) filters, in units of DN per sec per pixel. The temperature (T) and

the emission measure (EM) were computed using standard *Yohkoh* software (SXT-TEEM) which utilizes the filter ratio technique (Gerassimenko & Notle 1978; Hara et al., 1992).

In the optically thin corona, emission from the active region loops is mixed with a diffuse component. Therefore, calculations of the temperature usually require subtracting the background intensity from the images. For large data sets (as in our case), it is impractical to manually select the area with the background intensity in each image. Hence, here we defined the background as pixels with intensities less than 10% of the maximum brightness of both Al.1 and AlMgMn images in the same pair. Then the background was calculated (separately for Al.1 and AlMgMn images) as the average of all of the background pixels. To test this approach, we also calculated the background using a 5% intensity threshold. We did not find any noticeable difference in inferred temperatures, although in several cases the lower threshold resulted in the insufficient number of background pixels that could not be used for meaningful averaging.

3. Results

In Figure 1 we plot the calculated characteristics of the corona above active regions versus the magnetic power index (α). The plots show a significant correlation between the magnitude of the power index and the area-independent parameters of the soft X-ray emission. In all four cases, the steeper power spectra are associated with the brighter SXR emission, higher temperature and stronger emission measure in the corona.

In general, α is related to the intermittency of the magnetic field, i.e., α increases as the number of discontinuities in the magnetic field grows. Large α , therefore, implies the presence of a larger number of current sheets. Hence, Figure 1 may be interpreted as an indication that the brighter and hotter coronal emission may be associated with an increased number of current sheets, which can provide the energy necessary to heat the corona. This is in qualitative agreement with Fisher et al. (1998) who argued that the MCC model is the most probable mechanism of coronal heating. Note that Abramenko (2005) recently showed that steep power spectra are statistically associated with the high flaring productivity of active regions.

Figure 2 shows that a high magnetic energy dissipation rate is statistically correlated with strong X-ray flux, high temperature and high emission measure. The specific energy content in the hot corona above stable and decaying active regions seems to be proportional, under non-flaring conditions, to the specific energy of the footpoint motions in the photosphere. The observed correlation between the energy input due to the random motions and

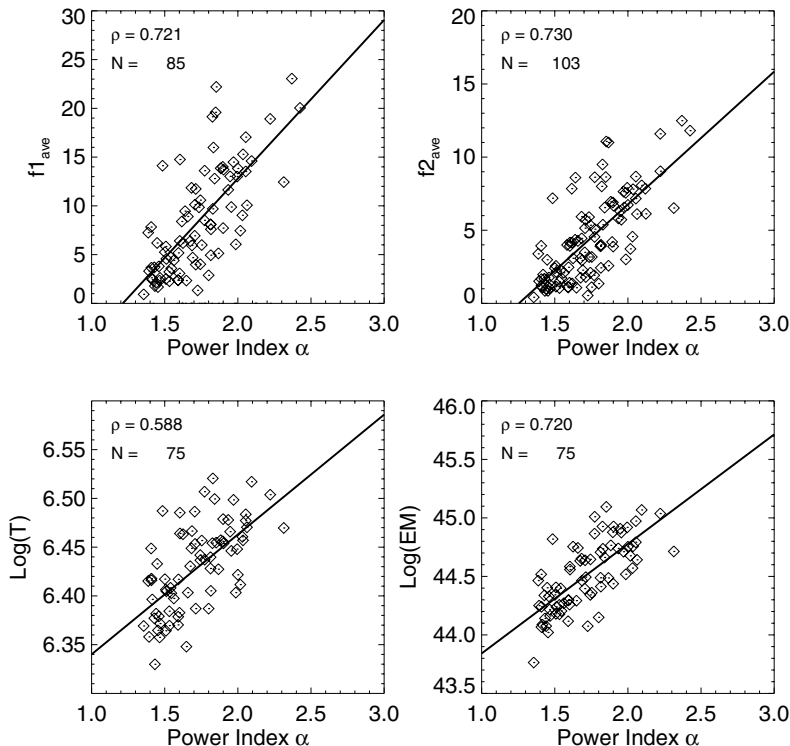


Fig. 1.— Power index α plotted versus the area-independent parameters of the coronal plasma such as the average SXR flux observed in Al.1 ($f1_{ave}$, *upper left*) and AlMgMn ($f2_{ave}$, *upper right*) filters; logarithm of temperature (*lower left*) and logarithm of emission measure (*lower right*). The corresponding correlation coefficients, ρ , and the statistics, N , are noted in each frame. Straight lines show the linear best fit to the data points. The averaged SXR flux is plotted in 10^2 DN per sec per pixel.

the brightness and temperature of the corona is a hallmark of coronal heating due to the twisting and braiding of magnetic flux tubes.

As we mentioned above (see Sec. 2.2), $\bar{\epsilon}$ represents the magnetic energy that was injected into the photosphere, at large scales (via, e.g., new flux emergence), cascaded toward smaller scales (via fragmentations) and eventually dissipated via resistivity at small scales. In this sense, Equations (2 - 4) allow us to estimate the magnetic energy flux injected into the photosphere that is related to the intensity of turbulent motions. Thus, the right-hand part of Eq. (3) was directly calculated for each of the 104 active regions, and the magnitude of $\bar{\epsilon}$, in the left-hand part, was evaluated from Eq. (4) by using the large-scale characteristics of an active region. For this purpose, we accepted that the typical size of an active region is about 100 Mm, while the typical increment of the transverse velocities in the photosphere

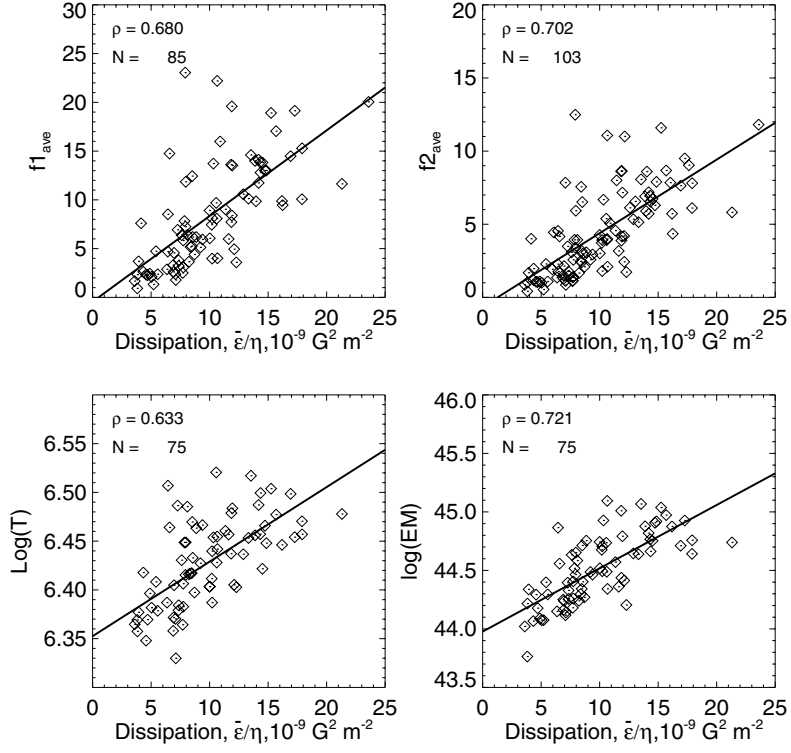


Fig. 2.— Magnetic energy dissipation rate $\bar{\epsilon}/\eta$ versus the area-independent parameters of the coronal plasma. Notations are the same as in Figure 1.

varies in the range of 0.5 – 1.0 km/s (Dere et al., 1990; Berger & Title 1996; Klimchuk 2006). The typical increments of B_z in an active region at spatial scales on the order of 100 Mm amounts to approximately 500G, as determined from calculations of the first-order structure functions (Abramenko et al., 2002). The magnitude of the unknown diffusion coefficient η in Eq. (3) is then approximately $\eta = (1.5 - 3) \times 10^8 \text{ m}^2\text{s}^{-1}$. Assuming that the effective thickness of the photosphere is about $h = 500 \text{ km}$, the inferred energy flux $\int \bar{\epsilon} dh$ for different active regions varies in the range of $(1 - 14) \times 10^6 \text{ erg cm}^{-2}\text{s}^{-1}$, which is sufficient to heat the X-ray corona (Withbroe & Noyes 1977).

4. Concluding remarks

In this study, the area-independent characteristics of the photospheric magnetic fields were compared to the soft X-ray luminosity of the corona above 104 active regions. The line-of-sight magnetic field data were obtained in the high resolution mode by the SOHO/MDI instrument, while the luminosity was inferred from *Yohkoh* Soft X-ray Telescope images

recorded within a 2 hour time window, centered at the moment of the corresponding MDI magnetogram. For the majority of active regions, the SXT data were available in two energy channels, which enabled us to determine coronal temperatures and emission measures.

The analysis showed that the soft X-ray flux, averaged over the active region, exhibits a strong correlation with i) the power index α of the magnetic power spectrum (Pearson correlation coefficient $\rho = 0.72$ for the Al.1 channel and 0.73 for AlMgMn channel) and ii) the magnetic energy dissipation rate $\bar{\varepsilon}/\eta$ [$\rho(\text{Al.1}) = 0.68$ and $\rho(\text{AlMgMn}) = 0.70$]. Both magnetic parameters also produced a significant correlation with the logarithm of emission measure ($\rho = 0.72$) and the logarithm of temperature ($\rho = 0.59-0.63$). These results indicate that the higher magnetic energy dissipation rate and the steeper magnetic spectra are related to the higher intensity of the coronal emission.

As long as $\bar{\varepsilon}$ is proportional to the horizontal velocity of magnetic field concentrations in the photosphere, we speculate that the intensity of random footpoint motions is related to the intensity of the soft X-ray corona, emission measure and temperature. Moreover, the estimated magnetic energy flux, related to the turbulent cascade in the photosphere, is about $(1 - 14) \times 10^6 \text{ erg cm}^{-2}\text{s}^{-1}$ and is quite sufficient to heat the corona above active regions. Since we did not directly measure transverse velocities, we cannot indicate the exact location of these intense random motions. Although one can assume that these motions take place in the photosphere, it is also possible that they might be tied to the turbulent flows below the photosphere. Results of this statistical study provide observational support for those theoretical models that employ random motions of magnetic flux tubes in the photosphere as a primary mechanism for coronal heating (e.g., Priest et al., 2002; Gudiksen & Nordlund 2002; Dahlburg et al., 2005; Klimchuk 2006 and references therein).

Eq. (1) postulates that the Poynting flux should be constant if there are no variations in B_t , B_v and V_t . In respect to the quiet Sun, both transverse displacements (due to convective motions) and the properties of the magnetic field (network fields) are not expected to change significantly from solar minimum to solar maximum. Therefore, the energy input to the corona should be independent of the phase of a solar cycle. Soft X-ray observations, however, show significant variations in the brightness of the quiet Sun's corona between solar minimum and maximum (e.g., Pevtsov & Acton 2001). To reconcile this apparent contradiction, we propose that the source of the overall brightness of the quiet Sun's corona, in the SXT temperature range, is dominated by the luminosity of active regions and large-scale coronal loops. The contribution of the random footpoint motion mechanism to the heating of the quiet Sun's corona may be significant at lower temperatures ($< 10^6 \text{ K}$) that were not well-observed by SXT on *Yohkoh*. Testing of this hypothesis would require near simultaneous high resolution magnetic and EUV/X-ray observations from future space missions (e.g. Solar-B

and Solar Dynamics Observatory).

The Yohkoh SXT was a collaborative project supported by NASA and ISAS. SOHO is a project of international cooperation between ESA and NASA. The National Solar Observatory (NSO) is operated by the Association of Universities for Research in Astronomy (AURA, Inc.) under cooperative agreement with NSF. V. Abramenko was supported, in part, by NASA NNG05GN34G grant.

REFERENCES

- Abramenko, V.I. 2005, *ApJ*, 629, 1141
- Abramenko, V.I., Yurchyshyn, V.B., Wang, H., Goode, P.R. 2001, *Solar Phys.*, 201, 225
- Abramenko, V.I., Yurchyshyn, V.B., Wang, H., Spirock, T.J., & Goode, P.R. 2002, *ApJ*, 577, 487
- Berger, T.E. & Title, A.M. 1996, *ApJ*, 463, 365
- Dahlburg, R.B., Klimchuk, J A., & Antiochos, S.K. 2005, *ApJ*, 622, 1191
- Dere, K.P., Schmieder, B., & Alissandrakis, C.E. 1990, *A&A*, 233, 207
- Fisher, G.H., Longcope, D.W., Metcalf, T.R., Pevtsov, A.A. 1998, *ApJ*, 508, 885
- Freeland, S. L., Handy, B. N. 1998, *Solar Phys.*, 182, 497
- Gerassimenko, M. & Nottle, J.T. 1978, *Solar Phys.*, 60, 299
- Gudiksen, B.W., Nordlund, A. 2002, *ApJ*, 572, L113
- Hara, H., Tsuneta, S., Lemen, J. R., Acton, L. W., & McTiernan, J.M. 1992, *PASJ*, 44, L135
- Klimchuk, J.A. 2006, *Solar Phys.* 234, 41
- Lundquist, L. L., Fisher, G. H., McTiernan, J. M., & Régnier, S. 2004, *ESA SP-575: SOHO 15 Coronal Heating*, 15, 306
- Longcope, D. 1996, *Solar Phys.*, 169, 91
- Monin, A.S., Yaglom, A.M. 1975, "Statistical Fluid Mechanics", vol. 2, ed. J.Lumley, MIT Press, Cambridge, MA

- Parker, E.N. "Cosmical magnetic fields, their origin and their activity", Oxford University Press, 1979
- Parker, E.N. 1988, ApJ, 330, 474
- Petrovay, K., Szakaly, G. 1993, A&A, 274, 543
- Pevtsov, A. A., & Acton, L. W. 2001, ApJ, 554, 416
- Pevtsov, A. A. et al. 2003, ApJ, 598, 1387
- Priest, E. R., Heyvaerts, J., & Title, A.M. 2002, ApJ, 576, 533
- Schrijver, C.J., Sandman, A. W., Aschwanden, M.J., DeRosa, M.L. 2004, Astrophys. J., 615, 512
- Schrijver, C. J., & Title, A. M. 2005, ApJ., 619, 1077
- Scherrer, P.H. et al. 1995, Solar Phys., 162,129
- Stenflo, J.O., Holzreuter, R. 2002, in: SOLMAG 2002, ESA SP-505, 101
- Tsuneta, S. et al. 1991, Solar Phys. 136, 37
- Withbroe, G.L., Noyes, R.W. 1977, ARA&A, 15, 363